International Journal for Housing Science and Its Applications
Publish August 10, 2025. Volume 46, Issue 4 Pages 1002-1013

https://doi.org/10.70517/ijhsa46493

Synergistic study of integrated smart toilet standardized module design and recycled concrete application for low carbon assembled toilet system

Huan Nie[1,*]
[1] Technology Department, Chongqing Technology and Business Institute, Chongqing Open University, Chongqing, 400052, China
Corresponding authors: (e-mail: niehuan2025@163.com).

Abstract Driven by the green building concept, assembly building technology has gradually become an important direction for the transformation and upgrading of the construction industry. At the same time, the development of construction waste recycling technology provides a new way to solve the problem of construction waste disposal, and the application of recycled materials in the assembly building system can not only reduce the construction cost, but also reduce the environmental load and realize the goal of sustainable development. In this paper, a synergistic efficiency system of low-carbon assembled toilet system is constructed by combining the standardized modular design of integrated smart toilets with the application of recycled concrete. The study used ABAQUS finite element software to establish a numerical simulation calculation model for the seismic performance of the energy-consuming combination wall, analyzed the performance of recycled concrete using the concrete damage plasticity model, and realized standardized production through the principle of modular design. The test results show that the ultimate load of the roof cover reaches 109.72kN, the initial stiffness is 4.5kN/mm, and the energy-consuming capacity of the KJ-6 node is 12.2 times higher than that of the empty steel frame. The technical and economic analysis shows that the total cost of Project A with recycled concrete composite thermal insulation blocks is 1055.14 yuan/m², which is 48.6% lower than that of traditional concrete Project B of 2054.72 yuan/m², and the thermal insulation cost only accounts for 1.36% of the total project budget. The study shows that the modular design of the integrated smart toilet combined with the application of recycled concrete significantly reduces the construction cost and improves the efficiency of resource utilization under the premise of ensuring the structural safety performance, which provides technical support and economic feasibility verification for the development of low-carbon assembled buildings.

Index Terms Integrated Smart Toilet, Standardized Module, Recycled Concrete, Low Carbon Assembly, Synergy, ABAQUS

I. Introduction

Toilet is an important public facility related to the life of urban and rural residents, the number is huge, but at present, the construction of urban and rural toilets still has problems such as waste of resources and high carbon emissions [1], [2]. In order to respond to the country's dual-carbon strategy goal, the construction industry needs to take the initiative. The design of assembled intelligent toilets that can realize self-supply of energy during operation can realize the low-carbon goal of "zero energy consumption" of buildings, thus making a positive attempt for the construction industry to respond to the national "dual-carbon" strategic goal [3]-[5].

The construction of multi-functional transformation space based on the integration of equipment with a collection of design-assisted units provides a new idea for the modernization of residential construction [6]. Modularization and integration not only represent prefabricated assembled buildings entering a higher stage of development, but also a significant feature in the process of construction industrialization [7], [8]. Standardized prefabricated module production not only ensures a high standard of building quality, but also enhances the efficiency of on-site construction through factoryization, which not only enhances the flexibility and adaptability of the building, but also extends its service life [9]-[11]. By disassembling the building and recycling the material components, the goals of resource conservation, environmental protection, and sustainable development are realized [12]-[14]. Based on this, the design of integrated smart toilet standardized modules based on new building technologies and assembly components can effectively improve the construction quality and sustainability of housing.

This study builds a technical system that combines the standardized module design of integrated intelligent toilet and the application of recycled concrete. Firstly, the modular design method of integrated intelligent toilet is established to realize the standardized production and assembly construction of the toilet system through the division of functional modules, standardized design of interfaces and optimization of component integration. Then ABAQUS finite element analysis software is used to establish a numerical simulation model of the seismic performance of the energy-consuming combination wall, and a concrete damage plasticity model is used to analyze the mechanical properties and damage characteristics of recycled concrete. Finally, the technical and economic analysis is carried out through actual engineering cases to verify the application effect and economic feasibility of recycled concrete in low-carbon assembled toilet system, which provides theoretical basis and practical guidance for the popularization of application.

II. Method

II. A. Modular Design of Integrated Smart Toilet

II. A. 1) Principles of modularization

The division of integrated intelligent toilet modules should comprehensively consider factors such as functional requirements, production and transportation convenience, and installation feasibility. Follow the principles of standardization and universality to improve the reuse rate of modules and reduce production costs. At the same time, ensure that the connection between the modules is reliable, watertight and airtight, so as to facilitate rapid assembly at the construction site. For example, integrated intelligent toilets can be divided into basic modules such as chassis, wall panels, roof panels, sanitary appliances, etc., which can be flexibly combined according to different building types and user needs.

II. A. 2) Interface design

Interface design is the key to ensure that the integrated intelligent toilet modules work together, including piping interfaces, electrical interfaces, structural connection interfaces and so on. The pipeline interface should adopt standardized quick-connect fittings to ensure smooth water flow and no leakage. The electrical interface should be reserved in an accurate position to facilitate the installation and maintenance of electrical equipment in the later stage. Structural connection interfaces should be designed with reasonable connection methods, such as bolt connection, card slot connection, etc., to ensure the connection strength and stability between modules.

II. A. 3) Component Selection and Integration

According to the functional requirements of the integrated intelligent toilet, select components with excellent performance and appropriate dimensions, such as water-saving sanitary appliances, high-efficiency air-exchange equipment, and waterproof and moisture-proof decorative materials. The integrated design of these components can optimize the spatial layout and improve the comfort of using the integrated intelligent toilet. For example, the use of integrated basins and toilets reduces hygienic dead ends and facilitates cleaning. Intelligent sensor-type faucets and lighting are selected to enhance the user experience.

II. B. Numerical simulation calculation model of seismic performance of energy-consuming combination wall

In this paper, ABAQUS was chosen for finite element analysis, which is perfectly suited to create an equal-scale finite element model of an energy-consuming modular wall. The correctness of the model created by finite elements can be proved by comparing the experimental phenomena and the modeled damage patterns from numerical simulations [15]. After that, the seismic performance and hysteresis characteristics of the energy-consuming modular wall are further understood and analyzed. The reliability of the structural simulation of the energy-consuming modular wall is demonstrated and the two lines of seismic defense are verified so that appropriate seismic design recommendations can be made for this structure.

II. B. 1) Material principal modeling

(1) Concrete constitutive relationship

ABAQUS commonly used concrete is mainly divided into three kinds of ontological models: concrete diffuse cracking model, concrete brittle cracking model and concrete damage plastic model. In this paper, the concrete plastic damage model is taken to simulate.

1) Concrete compression and tension damage

The plastic damage model of concrete in ABAQUS is based on the plastic damage model, assuming that the concrete material mainly has tensile cracking and crushing under pressure. Its yield and damage are determined by the equivalent tensile plastic strain $\tilde{\varepsilon}_t^{pl}$, equivalent compressive plastic strain $\tilde{\varepsilon}_c^{pl}$, respectively.

Concrete tensile damage curve is calculated by converting cracking strain into plastic damage strain through the relationship between destructive stress and cracking strain, while concrete compressive damage curve is calculated by further converting inelastic strain into plastic strain. The formulas for both calculations are shown in Eqs. (1) and (2):

$$\tilde{\varepsilon}_t^{pl} = \tilde{\varepsilon}_t^{ck} - \frac{d_t}{(1-d_t)}\frac{\sigma_t}{E_0} \tag{1}$$

$$\tilde{\varepsilon}_c^{pl} = \tilde{\varepsilon}_c^{in} - \frac{d_c}{(1-d_c)}\frac{\sigma_c}{E_0} \tag{2}$$

where, $\tilde{\varepsilon}_t^{ck}$ - the cracking strain, which is the total strain minus the elastic strain of the undamaged material, i.e., $\tilde{\varepsilon}_t^{dk} = \varepsilon_t - \varepsilon_0 t^{el}$, $\varepsilon_{0t}^{el} = \sigma_t / E_0$. $\tilde{\varepsilon}_c^{in}$ - the compressive inelastic strain, which is the total strain minus the elastic strain of the lossless material, i.e. $\tilde{\varepsilon}_c^{im} = \varepsilon_c - \varepsilon_{0c}^{el}$, $\varepsilon_{0c}^{el} = \sigma_c / E_0$, d_t - stretch damage variable, d_c - compression damage variable.

2) Concrete principal relationship

In this paper, the poured concrete compression eigenstructure equations are selected from the stress-strain relationship of concrete under uniaxial pressure proposed by the Code for the Design of Concrete Structures, see Eqs. (3)-(7):

$$\sigma = (1-d_c)E_c\varepsilon \tag{3}$$

$$d_c = \begin{cases} 1-\dfrac{\rho_c n}{n-1+x^n} & x \le 1 \\ 1-\dfrac{\rho_c n}{\alpha_c(x-1)^2+x} & x > 1 \end{cases} \tag{4}$$

$$\rho_c = \frac{f_{c,r}}{E_c\varepsilon_{c,r}} \tag{5}$$

$$n = \frac{E_C\varepsilon_{C,r}}{E_c\varepsilon_{C,r} - f_{C,r}} \tag{6}$$

$$\chi = \frac{\varepsilon}{\varepsilon_{c,r}} \tag{7}$$

α_c - parameter values of the descending section of the uniaxial compressive stress-strain curve of concrete, taken according to the table of concrete structure design code.

$f_{c,r}$ - representative values of uniaxial compressive strength of concrete, the values of which can be taken as f_c, f_{ck} or f_{cm}, respectively, according to the needs of actual structural analysis.

$\varepsilon_{c,r}$ - peak compressive strain of concrete corresponding to uniaxial compressive strength $f_{c,r}$, taken from the table of structural design codes for concrete.

d_c - damage evolution parameters for uniaxial compressive strength of concrete.

The concrete tensile principal model assumes that there is no damage before the concrete reaches the peak stress, and the curves of the descending section are calculated according to Eqs. (8)-(11).

$$\sigma = (1-d_t)E_c\varepsilon \tag{8}$$

$$d_t = \begin{cases} 1-\rho_t[1.2-0.2x^5] & x \le 1 \\ 1-\dfrac{\rho_t}{\alpha_t(x-1)^{1.7}+x} & x > 1 \end{cases} \tag{9}$$

$$x = \frac{\varepsilon}{\varepsilon_{t,r}} \tag{10}$$

$$\rho_t = \frac{f_{t,r}}{E_C\varepsilon_{t,r}} \tag{11}$$

α_t - parameter value of descending section of uniaxial tensile stress-strain curve of concrete, which is taken according to the table of concrete structure design code.

$f_{t,r}$ - representative values of uniaxial tensile strength of concrete, the values of which can be taken according to the needs of actual structural analysis as f_t, f_{tk} or f_{tm} respectively.

$\varepsilon_{t,r}$ - peak compressive strain of concrete corresponding to uniaxial compressive strength $f_{t,r}$, taken from the table of structural design codes for concrete.

d_t - concrete uniaxial tensile strength damage evolution parameters.

(2) Steel principal model

In this paper, both steel reinforcement and steel plate are modeled by bifolds, the yield criterion is Mises yield criterion, and the strengthening criterion is the following strengthening criterion [16]. The true values of stresses and strains are used in ABAQUS software, while the material tensile tests are measured as nominal stresses σ_{nom} and nominal strains ε_{nom}. They can be transformed by equations (12) and (13):

$$\varepsilon = \ln(1+\varepsilon_{nom}) \tag{12}$$

$$\sigma = \sigma_{nom}(1+\varepsilon_{nom}) \tag{13}$$

(3) Structural damage model

In this paper, the plastic damage model (CDP) is used to reflect the plastic deformation and damage of concrete materials. In the plastic damage model, the damage index D_w of concrete can be calculated by Eq. (14), while the damage index D_F of steel frame can be calculated by Eq. (15). Concrete wall panels are mainly affected by tensile stresses under horizontal loading, i.e., evaluated by D_w, and they are mainly affected by axial compressive stresses due to the horizontal restraining effect of the steel tubes on the concrete inside them, i.e., evaluated by D_F:

$$D_W = 1-\frac{\sigma_t}{E_0(\varepsilon_t-\varepsilon_t^{pl})} \tag{14}$$

$$D_F = 1-\frac{\sigma_C}{E_0(\varepsilon_C-\varepsilon_C^{pl})} \tag{15}$$

In Equation (14) σ_t is the tensile stress, ε_t is the tensile strain, ε_t^{pl} is the tensile elastic strain, and E_0 is the initial elastic modulus. In Equation (15) σ_c is the compressive stress, ε_c is the compressive strain, ε_c^{pl} is the compressive elastic strain, and E_0 is the initial elastic modulus.

II. B. 2) Unit Module Selection

First of all, in the “part” module, according to the specimen's actual geometric dimensions of the specimen, respectively, the structure of the components of the proportional modeling, including: thin-walled square steel tube beams and columns and the internal injection of concrete, concrete sheet walls, bidirectional distribution of reinforcing steel, linking steel, loading head, loading beams and so on. After the model of each part is established, each part is assembled into a whole in the “assembly” module to obtain a model consistent with the actual test. The constraints used are mainly “Tie”. The loading beams are used to apply vertical loads uniformly at the ends of the external frame columns by simulated jacks. The loading head is to simulate the loading of the member by the horizontal actuator. The square steel pipe columns and beams, steel pipe filled concrete, and wall panel concrete are simulated using the converged C3D8R unit in the software, the distributed reinforcement adopts the T3D2 unit, and the connecting nodes of the beams and columns, and the steel plate sheet connected to the concrete slab in the frame adopt the S4R unit. The combination of each module of the model is shown in Figure 1.

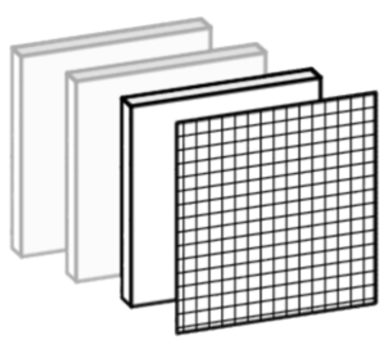

Figure 1: Model module combination

II. C. Creation of Finite Element Models

II. C. 1) Creation of structural component models

Based on the geometry of the specimen, the structural components were modeled, mainly including: steel pipe filled with recycled concrete, square steel pipe of border beam and column, recycled concrete wall, steel reinforcement and mesh frame, horizontal load loading head and distribution beam. In order to simplify the model and improve the computational efficiency, the high-strength bolts with stiffened ribbed plate reinforced nodes and column footing connected to the foundation steel are omitted from the model, after which the binding constraints are equated to a rigid connection. Distribution beams are used in order to distribute the vertical loads uniformly on both sides of the tubular concrete columns in the simulation and to avoid stress concentrations [17]. The loading head is used in order to avoid stress concentration at the loading location for horizontal loads. The square steel tubes of the frame beams and columns, the concrete filled in the steel tubes, and the concrete wall panels are all simulated using the C3D8R eight-node 3D solid unit, which is based on the hexahedral linear reduced integration mode, and the reduced integration reduces the number of integration points in the unit, which can avoid the occurrence of shear self-locking phenomenon under the bending load and improve the rate of computation when compared with the 3D linear integration unit (C3D8). In the simulation dominated by shear deformation, the use of C3D8R cell is more efficient than the second-order cell or the first-order non-decreasing integral cell, and in the case of mesh distortion and deformation, the reasonable subdivision of the mesh can improve the accuracy with little effect. The reinforcement in the wall panel is modeled by T3D2 two-node 3D truss cell, which has only translational degrees of freedom at the nodes, and is subjected to tensile and compressive loads only, and the transverse shear strength can be neglected. The steel reinforcement is modeled using a split method, i.e., each rebar is modeled individually, and then the rebar is incorporated into the wall panel using an embedded form, so that the bond slip between the rebar and the wall panel concrete is not considered. The steel side frames within the recycled concrete wall panels are modeled using the S4R four-node general purpose shell unit, this solid unit is based on a reduced integral mode that allows for transverse shear deformation, and the general purpose shell unit takes into account finite membrane strains and arbitrarily large rotations, making it suitable for large-strain analyses.

II. C. 2) Creating materials, section properties and defining assemblies

Materials are created according to the ontological relationship between steel and recycled concrete, and concrete and steel are created separately. Set the elasticity in the mechanical properties of concrete material as isotropic, enter the modulus of elasticity and Poisson's ratio, select the concrete damage plasticity model for plasticity, define the plasticity properties, compression properties and tensile properties, and define the concrete compression damage model. In steel, the mechanical properties of elasticity are set to isotropic, the modulus of elasticity and Poisson's ratio are entered, and plasticity defines the relationship of yield stress-plastic strain. After that sections are created and components are given section properties [18].

II. C. 3) Defining boundary constraints

In order to simulate the horizontal and vertical loads on the combined structure in the experiment, the vertical and horizontal forces are applied by setting two reference points RP1 and RP2 in the simulation. Among them, the reference point RP1 for applying the vertical force is above the top center of the rigid distributed beam, and the axial load is applied by preserving the degree of freedom in the upper end direction through the boundary conditions to ensure that the point and direction of the applied vertical load remain unchanged in the experiment. Horizontal displacements are transferred by the large stiffness loading end to achieve simple and clear forces in the loading process. For the reference point RP2 where the horizontal load is applied, the reference point and the loading end have the same degree of freedom through coupling constraints to improve the convergence of the model analysis. The bottom surface of the model is defined as consolidation, and a fixed constraint ENCASTRE is set at the bottom of the two steel-tube concrete columns of the model to simulate the fixation of the members with the foundation.

II. C. 4) Gridding

ABAQUS provides three meshing methods: structured optimized meshing, swept meshing, and free meshing. In this paper, the model construction is simple, and in order to improve the accuracy, all the entities are meshed with hexahedral structured meshing, and the shell cells are meshed with tetrahedral-body cells free meshing. The seed density of wall meshing for this experimental finite element model is 50mm.

III. Results and discussion

III. A. Recycled concrete performance test experiment

III. A. 1) Destruction characteristics

At the early stage of loading, the specimen was in the linear elastic working state, the load increased linearly with displacement, and minor cracks appeared in the self-tapping nail set blocks at the bottom of the plate, without obvious damage phenomenon. When loaded to about 55% of the peak load, the stiffness of the specimen decreased significantly, the mid-span deformation of the plate reached 27.4 mm, and a number of long and thin diagonal cracks appeared at the bottom of the plate in the direction of 45°, with the starting point at the loading point and the end point at the corner of the plate, and the width of the cracks at the tapping nails collector block was carried out up to 1 mm. when loaded to the peak load, the compression crack appeared at the top of the plate in the mid-span of the counter beam, and the diagonal cracks appeared at the end part. The mid-span deformation of the roof cover increased to 81.6 mm. The cracks at the bottom of the slab continue to develop, overall along the plastic strand. When the load drops to about 85% of the peak load, the width of the penetrating crack of the self-tapping nail aggregate reaches 12 mm, the longitudinal reinforcement in the middle span of the anti-beam is obviously buckled, the concrete at the anti-beam has spalling, the roof is obviously bent and deformed downward, the crack at the bottom of the slab develops along the direction of the plastic hinge, and the crack at the top of the slab is distributed in an elliptical shape along the middle anti-beam. The steel beams, steel columns, and π-type joints were not significantly deformed.

III. A. 2) Deformation curves

The deformation curves are shown in Fig. 2 (Fig. a is the mid-span load-deflection curve, Fig. b is the deflection at each point in the plate in the direction of 4.5 m, and Fig. c is the comparison of deformation at the edge peg connection). The slope of the load-deformation curve decreases, the load growth is slow but the deformation growth is accelerated, plastic deformation occurs in the roof, and the bottom crack development is distributed as a plastic hinge line. c. Destruction stage, at this time, the concrete at the bottom of the slab has been cracked in a large area, and the tensile reinforcement in the span yields, and the load carrying capacity of the roof decreases drastically, and the growth of the deformation slows down. In Fig. (b), when the load increases to 99kN, the deflection of the roof cover suddenly increases and the stiffness decreases. Figure (c) shows the deformation of roof cover and steel beam at the edge of the peg connection comparison, in the vertical force increased to 55kN before the edge of the roof cover and the steel beam deformation is the same, after 55kN, the edge of the roof cover deformation gradually increased, while the steel beam is still not deformed, combined with the phenomenon of the test and the analysis of the characteristics of the point, the two appear to be different for the roof cover to reach the cracking load, at this time, the connection of the pegs will be weakened to a certain extent! However, the deformation difference between the two is only about 3mm, which is almost negligible.

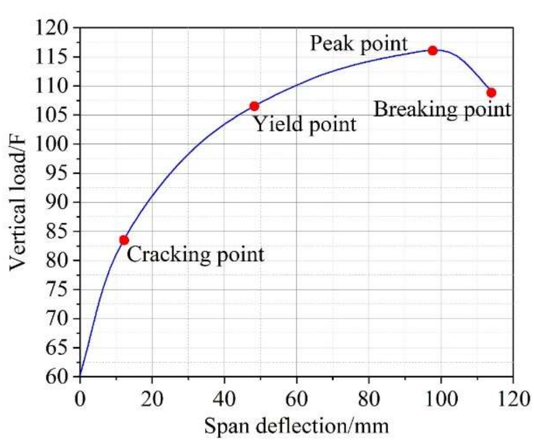

(a) Span load- Deflection curve

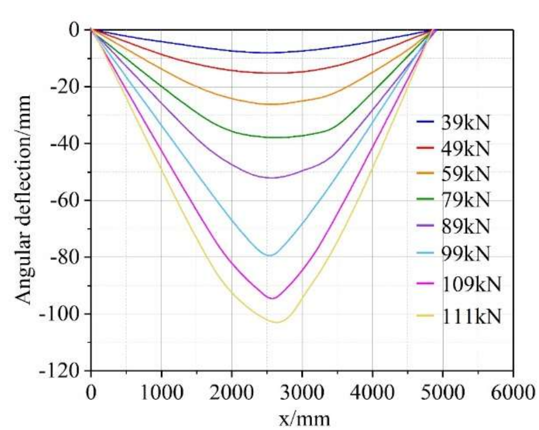

(b) Deflection of each point in the 4.5m direction plate

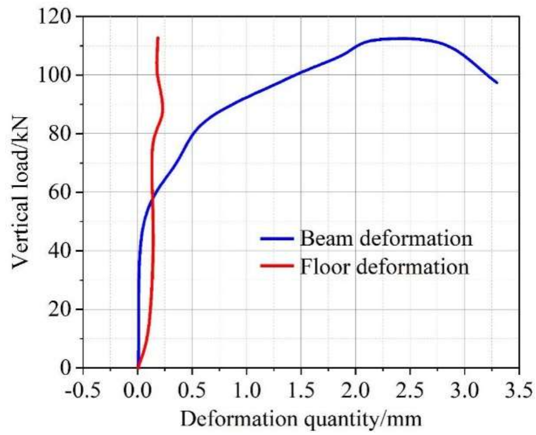

(c) Contrast of the junction of edge pin

Figure 2: Deformation curve

The measured characteristic values of the specimens are shown in Table 1. In the table, Fcr, Fy, Fm and Fd are the cracking load, yielding load, ultimate load and damage load of each specimen, respectively. Δcr, Δy, Δm and Δd are the relative cracking displacement, yielding displacement, peak displacement and damage displacement. From the table, the ultimate load of the roof cover can reach 109.72kN.

Table 1: Test feature value

Specimen name	Cracking point		Yield point (energy method)		Peak load point		Breaking point	
	Fcr/kN	Δ_{cr} / mm	Fy/kN	Δ_y / mm	Fm/kN	Δ_m / mm	Fd/kN	Δ_d / mm
Roof cover	52.4	21.77	91.85	46.24	109.72	94.82	95.71	117.87

III. A. 3) Stiffness

The cutline stiffness of the specimen is expressed as the ratio K of the vertical concentrated load carried by the specimen to the corresponding nominal mid-span deflection. The stiffness degradation process is shown in Fig. 3. As shown in the figure, the initial stiffness value of the roof cover is 4.5kN/mm, and the initial stiffness of the specimen is affected by various aspects such as the thickness of the plate and the connection method of the plate and strip, etc. The greater the thickness of the plate and the tighter the connection method of the plate and strip, the greater the initial stiffness. The stiffness degradation process of the roof cover can be divided into stiffness fast-declining stage and stiffness slow-declining stage. Combined with Table 1, before the specimen reaches the yield displacement, the specimen is in the stiffness fast-declining stage, and with the yielding of the tensile reinforcement and the penetration of the cracks at the tapping nail collector block, the stiffness decline slows down.

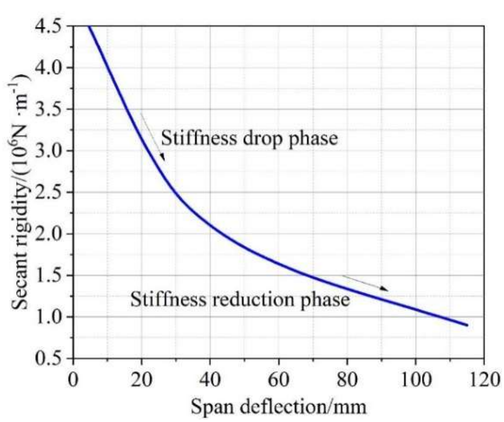

Figure 3: Stiffness degeneration process

III. A. 4) Strain characterization

The strain characteristics are shown in Fig. 4 (Fig. a shows the mid-span reinforcement strains, Fig. b shows the π-shaped node strains, Fig. c shows the bottom strains of the steel girder in the mid-span, and Fig. d shows the self-tapping nails collector block plate strains).From Fig. (a), it can be seen that all the mid-span distributed reinforcement at the bottom of the slab yielded, and the tension reinforcement at the bottom of the slab was fully stressed. Figure (b) can be seen, π shaped node of the lower π limbs subjected to pressure, the upper π limbs subjected to tensile, but are not up to the yield strength of the steel, there is no obvious damage, the cover meets the “strong node” design requirements, node connection is reliable. When the roof has a large deformation, the node has no deformation, indicating that the deformation of the roof will not affect the overall safety of the frame. From Figure (c), it can be seen that the steel beam has not reached the yield strength, combined with the test data, the bottom of the steel beam deformation is small, according to the above conclusions, the nodes and beams and columns together composed of the structural system deformation is small, almost negligible, the structural integrity is good. Figure (d) can be seen, self-tapping nails set block force transfer steel plate before reaching the peak load did not reach the yield strain, which indicates that the self-tapping nails set block connection can be achieved “strong node”, after the end of the test self-tapping nails set block of the steel plate did not occur obvious deformation, the connection is reliable.

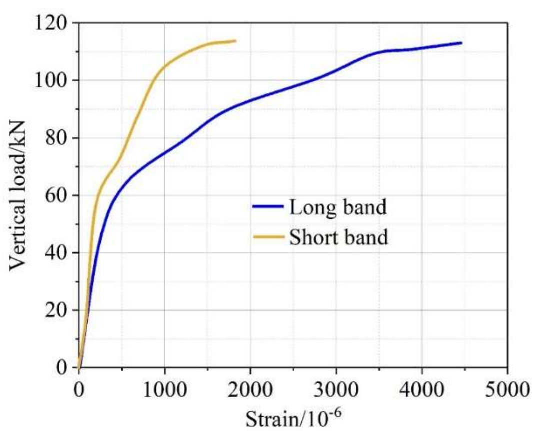

(a) Cross medium steel reinforcement strain

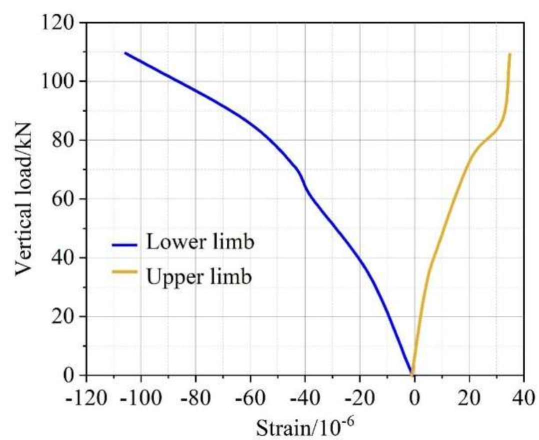

(b) Node strain

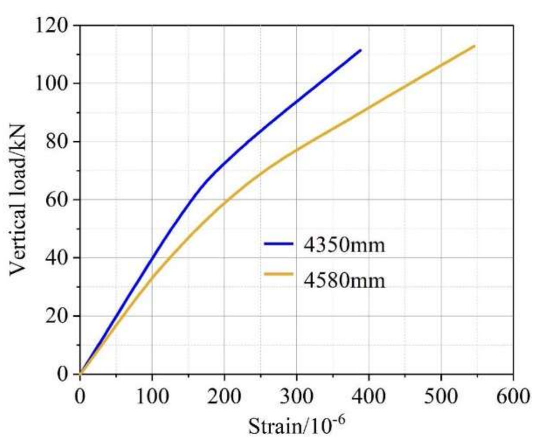

(c) Beam cross

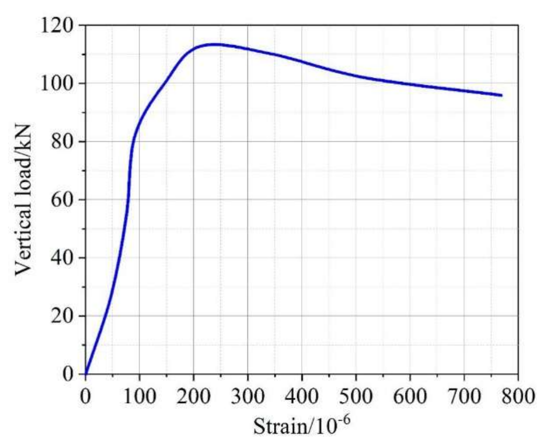

(d) Self-tapping nail set plate strain

Figure 4: Strain characteristic

III. B. Optimized design

III. B. 1) Energy consumption analysis

The energy consumption curves of the three specimens were obtained by simulation with ABAQUS limited element software. The energy dissipation curves of each specimen are shown in Fig. 5 (Figs. a~c show the energy dissipation curves of MX-1, MX-2 and MX-3, respectively). The empty steel frame (MX-1) has the worst energy dissipation capacity, and the channel steel-type nodes, angle steel-type nodes, straight plate-type nodes, reinforced nodes, and KJ-6 nodes are increased by 4.5, 4.6, 5.2, 6, and 12.2 times, respectively, compared with the empty steel frame. It can be seen that channel steel type nodes contribute little to the energy consumption of steel pipe concrete frames, reinforced nodes contribute much to the energy consumption of the frames, and increasing the size of beams and columns can significantly improve the energy consumption capacity of the structure.

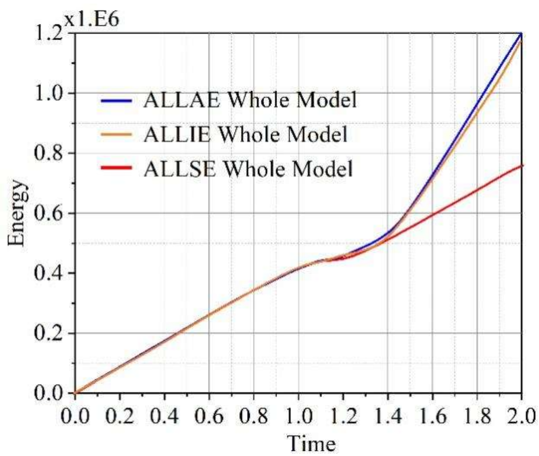

(a) MX-1

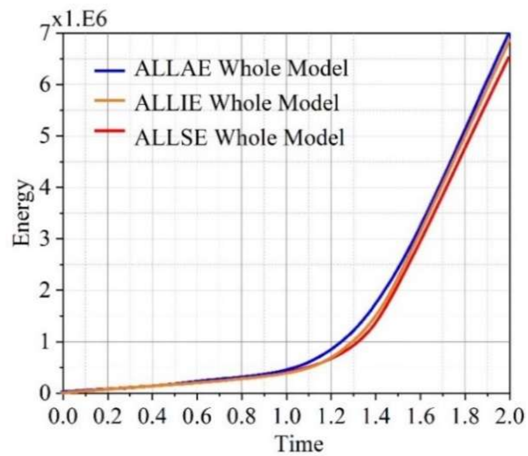

(b) MX-2

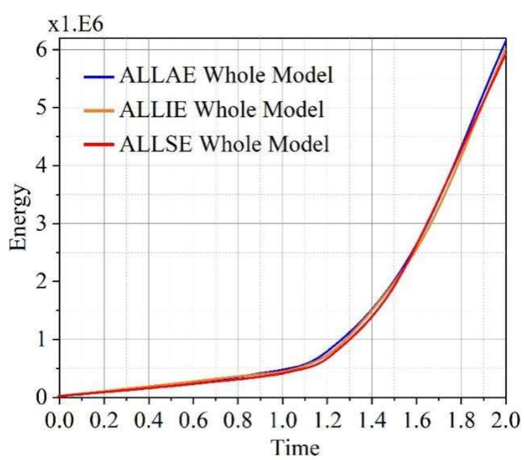

(c) MX-3

Figure 5: Each test is consumed by a graph

III. B. 2) Dimensional effects

Take MX-2 as an example to compare the model cloud diagrams under different beam-column sizes.The stiffening ribs at the beam-column nodes in MX-2 are all warped and deformed. The damage at the column footing and node locations is more obvious, and the tearing range of the MX-2 steel tube is larger during damage. Increasing the beam-column cross-section size by 40% for the frame structure including the node locations, the damage is reduced.

III. B. 3) Concrete strength effects

The unfilled lightweight steel frame has a slight warping deformation in the middle of the frame beam, bulging deformation and concave deformation at the column footing, and large stresses at the beam-column nodes and foundation joints under the low circumferential repeated loads. C40 recycled concrete is filled in the square steel pipe to form an assembled square steel pipe concrete structure. Comparing with the cloud diagram of the unfilled recycled concrete model, it can be clearly found that the damage of the structure is reduced, the node location is more obvious, and the bulging deformation of the foot of the columns is reduced in the degree and the range of deformation. The C50 recycled concrete inside the square steel pipe, compared with the C40 recycled concrete, can be seen to increase the strength of the recycled concrete, the stress of the structure increases, under the same displacement angle, the C50 concrete is subjected to a greater horizontal load, and the damage and deformation of the damage is small, which indicates that the filling of high-strength concrete can improve the shear and bending resistance of the structure.

III. C. Application of recycled concrete in low carbon fitted toilet systems

III. C. 1) Project description

This project is a community low carbon assembly toilet project A. The total construction area of the project is 45m² total 1 layer, through the BIM technology two-dimensional drawings for three-dimensional model perfect restoration, improve the quality of the design, guide the production and construction.

III. C. 2) Techno-economic analysis

(1) Comparative analysis of project profiles

In a community assembly project A, recycled concrete is used to build heat-insulating walls, and a commercial and residential building B is found to be similar to this design in terms of structural type, floor area, and other information, and the walls are made of traditional concrete. In order to detect the application of recycled concrete in cost control, a techno-economic analysis of projects A and B is conducted. A comparison of the project engineering profile is shown in Table 2.

Table 2: Comparison of project projects

project	A	B
Total floor area/m²	45	50
Building height/m	4	4
Building number	Layer 1	Layer 1
Earthquake intensity	Seven degree	Seven degree
Structural form	Frame shear structure	Frame structure
Basic type	Foundation foundation	Foundation foundation
Design life	Sixty years	Sixty years

(2) Comparative analysis of bidding control price

The main economic and technical indicators of the constructed project are shown in Table 3. It can be seen that the total cost of the similar project is 17630506.5 yuan, and the total cost is 2054.72 yuan/m², of which, the cost of the construction project is 1222.63 yuan/m², and the cost of the decoration project is 832.09 yuan/m².

Table 3: The main economic and technical indicators of the construction process

Sub-Item Name	Major Engineering And Technical Indicators		Sub-Economic Indicators		
	Project Cost/Yuan	Single Party Cost/(Yuan/M²)	Sub-Project	Branch Project Fee/Yuan	Total Cost Ratio/%
Construction Process	10445324.5	1222.63	Stonework	1200325.5	6.91
			Piling	92455.3	0.35
			Masonry Engineering	902531	5.19
			Concrete And Reinforced Concrete	5825412	39.64
			Roof And Waterproof Engineering	219275	1.02
Decorative decoration	7185182	832.09	Doors And Windows Engineering	380735.5	2.36
			Wall Engineering	3079641.5	17.66

			Floor Engineering	2049522.5	11.75
			Insulation	1285386.3	7.37
			Canopy Engineering	275551.5	6.4
			Scaffolding Engineering	247465.5	1.32
			Other Works	16151.7	0.03
Total	17630506.5	2054.72		15574453.3	100

In order to form a comparison with similar projects, according to the data available in similar projects, but also the relative price of the project has been summarized and organized, the main economic and technical indicators of the project as shown in Table 4. As can be seen from Table 3 and Table 4, Project A utilizes recycled concrete composite heat preservation blocks, and its thermal insulation, heat preservation cost in the project only occupies 1.36% of the total project budget. The use of recycled concrete composite thermal insulation blocks effectively reduces the project budget.

Table 4: Major economic and technical indicators of the project

Sub-Item Name	Major Engineering And Technical Indicators		Sub-Economic Indicators		
	Project Cost/Yuan	Single Party Cost/(Yuan/M²)	Sub-Project	Branch Project Fee/Yuan	Total Cost Ratio/%
Construction Process	5623374.3	560.02	Stonework	696614.55	6.45
			Piling	53676.41	0.61
			Masonry Engineering	659016.49	6.04
			Concrete And Reinforced Concrete	4168034.35	39.39
			Roof And Waterproof Engineering	47602.28	0.44
Decorative decoration	4959724	495.12	Doors And Windows Engineering	646945.31	6.23
			Wall Engineering	1962857.22	18.42
			Floor Engineering	1323718.42	12.41
			Insulation	185466.65	1.66
			Canopy Engineering	705 651.49	6.48
			Scaffolding Engineering	114814.32	1.63
			Other Works	20992.899	0.24
Total	10583098.3	1055.14		135807.2	100

IV. Conclusion

The synergistic research on the standardized module design of integrated smart toilet and the application of recycled concrete in this paper has achieved remarkable results. The finite element analysis results confirm that recycled concrete shows good mechanical properties in the low-carbon assembled toilet system, the roof structure shows good bearing capacity and deformation characteristics under vertical load, the damage process goes through three obvious stages of elasticity, elastoplasticity and damage, and the structural safety is effectively guaranteed. The application of KJ-6 reinforced nodes makes the energy consumption capacity of the steel-tube concrete frame significantly improved compared with that of the empty steel frame, which proves that the node design is optimized and the energy consumption capacity of the steel-tube concrete frame is improved. The application of KJ-6 reinforced nodes makes the energy-consuming capacity of steel pipe concrete frame compared with that of empty steel frame significantly improved, which proves the important influence of node design optimization on the overall structure performance.

The technical and economic analysis shows that the application of recycled concrete composite heat preservation blocks brings significant economic benefits, and the total project cost control effect is obvious, with outstanding cost advantages. The implementation of the modular design concept effectively improves the production efficiency and construction quality, and the standardized interface design ensures reliable connection and good sealing performance between the modules. The application of recycled concrete materials not only meets the structural strength requirements, but also realizes the resourceful utilization of construction waste, which is in line with the development concept of green building and circular economy. This technical system provides a successful example for the popularization and application of assembly building in the field of public facilities, and is of great significance in promoting the transformation and upgrading of the construction industry and sustainable development.

Funding

This work was supported by the Science and Technology Research Program of Chongqing Municipal Education Commission (Grant No.KJQN202404023).

References

[1] Yan, R., Cheng, S., Chen, J., Li, X., Sharma, S., Uddin, S. M. N., ... & Wang, X. (2021). Operating status of public toilets in the Hutong neighborhoods of Beijing: An empirical study. Journal of environmental management, 287, 112252.

[2] Haines-Gadd, M., Hasegawa, A., Hooper, R., Huck, Q., Pabian, M., Portillo, C., ... & McBride, A. (2015). Cut the crap; design brief to pre-production in eight weeks: Rapid development of an urban emergency low-tech toilet for Oxfam. Design Studies, 40, 246-268.

[3] Cheng, S., Ye, Z., Li, X., Manga, M., Dorea, C., Chen, Z., ... & Li, T. (2024). Constructing a toilet standard system for the toilet revolution in China. Journal of Water, Sanitation and Hygiene for Development, 14(4), 291-301.

[4] Morelli, M., & Brandt, E. (2016). A performance assessment of prefabricated bathrooms installed in the 1990s. Recent developments in building diagnosis techniques, 105-126.

[5] Cheng, C., Gao, R., Xu, G., Liu, J., & Ran, K. (2022, February). Research on prefabricate-decoration integration technology based on prefabricated bathroom. In IOP Conference Series: Earth and Environmental Science (Vol. 983, No. 1, p. 012105). IOP Publishing.

[6] Barbu, A. F., & Bârsan, L. (2022). Study on Designing a Modular House. Bulletin of the Transilvania University of Brasov. Series I-Engineering Sciences, 15-22.

[7] Dara, C., & Hachem-Vermette, C. (2019). Evaluation of low-impact modular housing using energy optimization and life cycle analysis. Energy, Ecology and Environment, 4(6), 286-299.

[8] Hachem-Vermette, C., Dara, C., & Kane, R. (2018). Towards net zero energy modular housing: a case study. Modular and Offsite Construction (MOC) Summit Proceedings.

[9] Laovisutthichai, V., Lu, W., & Xue, F. (2020, November). Modular construction: Design considerations and opportunities. In International Symposium on Advancement of Construction Management and Real Estate (pp. 1351-1361). Singapore: Springer Singapore.

[10] Da Rocha, C. G., Formoso, C. T., & Tzortzopoulos, P. (2015). Adopting product modularity in house building to support mass customisation. Sustainability, 7(5), 4919-4937.

[11] Kamali, M., Hewage, K., & Sadiq, R. (2019). Conventional versus modular construction methods: A comparative cradle-to-gate LCA for residential buildings. Energy and Buildings, 204, 109479.

[12] Tembhurkar, S., Ralegaonkar, R., Azevedo, A., & Madurwar, M. (2022). Low cost geopolymer modular toilet unit for ODF India–A case study. Case Studies in Construction Materials, 16, e00937.

[13] Clement, F. D., Qidong, L., Xingwen, Z., & Xiaojuan, L. (2022). Studies on Modular Emergency Buildings and Conservation. American Journal of Civil Engineering and Architecture, 10(1), 57-64.

[14] Oorschot, L., & Asselbergs, T. (2021). New housing concepts: Modular, circular, biobased, reproducible, and affordable. Sustainability, 13(24), 13772.

[15] Chunming Xu,Mingchao Yu & Hao Wu. (2018). Simulation Analysis of Quenching Process of High Strength Steel Based on ABAQUS. IOP Conference Series: Materials Science and Engineering,423(1).

[16] Dong Sun,Xudong Yang,Hui Liu & Hai Yang. (2025). BESO Topology Optimization Driven by an ABAQUS-MATLAB Cooperative Framework with Engineering Applications. Applied Sciences,15(9),4924-4924.

[17] Daniel de Lima Araújo,Guilherme de Paula Lisboa & Arthur Álax de Araújo Albuquerque. (2025). A reduced-order finite element model for the analysis of RC floor buildings under column loss. Engineering Structures,336,120434-120434.

[18] Jian Sheng Fan,Mu Nan Xu,Yan Chang Li,Yi Fan Ding,Yu Fei Liu,Bin Geng & Xin Jun Liao. (2025). Mechanics-based digital twin model for structural construction using 3D scanning and FE model updating. Automation in Construction,173,106109-106109.